

Investigation of Thirty Meter Telescope Wavefront Maintenance Using Low Order Shack-Hartmann Wavefront Sensors to Correct for Thermally Induced Misalignments

Carl Nissly^{a,b}, Byoung-Joon Seo^{a,b}, Mitchell Troy^{a,b}, George Angeli^c, Myung Cho^c,
Chris Shelton^{a,b}, Norbert Sigrist^{a,b}, Mark Sirota^c

^aJet Propulsion Laboratory, Pasadena, CA. 91109, USA

^bCalifornia Institute of Technology, CA. 91125, USA

^cThirty Meter Telescope Observatory, CA. 91107, USA

ABSTRACT

We evaluate how well the performance of the Thirty Meter Telescope (TMT) can be maintained against thermally induced errors during a night of observation. We first demonstrate that using look-up-table style correction for TMT thermal errors is unlikely to meet the required optical performance specifications. Therefore, we primarily investigate the use of a Shack-Hartmann Wavefront Sensor (SH WFS) to sense and correct the low spatial frequency errors induced by the dynamic thermal environment. Given a basic SH WFS design, we position single or multiple sensors within the telescope field of view and assess telescope performance using the JPL optical ray tracing tool MACOS for wavefront simulation. Performance for each error source, wavefront sensing configuration, and control scheme is evaluated using wavefront error, plate scale, pupil motion, pointing error, and the Point Source Sensitivity (PSSN) as metrics. This study provides insight into optimizing the active optics control methodology for TMT in conjunction with the Alignment and Phasing System (APS) and primary mirror control system (MICS).

Keywords: Wavefront Sensing and Control, Active Optics, On-Instrument Wavefront Sensor, Shack-Hartmann, Segmented Mirrors, Optical Modeling, MACOS, Point Source Sensitivity, Thirty Meter Telescope

1. INTRODUCTION

Environmental effects can have a significant impact on telescope wavefront quality. The science requirements for the Thirty Meter Telescope (TMT) demand a pristine wavefront quality, which necessitates careful consideration of misalignments induced from temperature gradients across the mirror elements and telescope structure. Despite careful environmental control of telescope enclosure temperature and wind speed, the TMT thermal and structural models predict micron and microradian level motions of mirror elements over the course of an observation night. Over a typical night, these motions induce approximately $7\mu\text{m}$ rms wavefront error and a Point Source Sensitivity (PSSN)¹⁻³ of 0.35, this implies a 65% loss in image performance from thermal misalignment alone.

To correct for this significant wavefront error, one can imagine the use of temperature sensors and a look-up-table (LUT) method of maintaining the telescope alignment to an acceptable level. We conclude that meeting the current TMT requirements and implementing this method would be challenging. As a preliminary calculation we consider a LUT that can measure the temperature accuracy to $\sim 0.05^\circ\text{C}$ per $^\circ\text{C}$ (5% temperature knowledge error) along the optical axis to correct for only the misalignment along the M2 piston direction. This would correct the telescope image quality to a PSSN of 0.991, which already falls below the requirement of 0.996. This considers only the simplest degree-of-freedom (DoF) to correct and does not yet include temperature distribution measurements across transverse directions at M1 or M2. Due to this level of precision of required temperature knowledge throughout the telescope structure, many large telescopes employ an active optics control strategy to maintain image quality.

Further author information: (Send correspondence to Carl Nissly) E-mail: Carl.R.Nissly@jpl.nasa.gov

A low order Shack-Hartmann wavefront sensor (SH WFS) can measure large amounts of wavefront error caused by system misalignment and provide the information necessary to correct for these errors and maintain the required image quality. This study investigates how well a SH WFS can maintain the wavefront when co-mounted with a science instrument using a guide star to measure the wavefront, this we refer to as an On-Instrument Wavefront Sensor (OIWFS).

Here we describe the simulation framework and current findings of our studies, separating apart the explanation as follows. Section 2 characterizes the system disturbance inputs from TMT thermal and structural modeling. Section 3 describes the optical, OIWFS, and atmospheric noise models used to simulate the TMT wavefront. In Section 4 we describe the wavefront control methodology and optical metrics used to evaluate wavefront performance. The baseline simulation case and performance statistics are reported in Section 5 and parameter studies used to determine these baseline simulation conditions are described in Section 6.

2. SYSTEM DISTURBANCES

2.1 Thermal Environment

The thermal misalignment disturbances used as an input to this OIWFS simulation are derived from a thermal and structural modeling activity for the TMT. This extensive model captures conduction, convection, and radiation effects from three operational days and nights recording temperatures and rigid-body state for points on each mirror, instrument, and around the enclosure.^{4,5} An 11.5 hour time series for each night is passed to the optical model for 492 M1 segments, M2, and M3. Night 1 is a thermal transient to steady operational state, while Night 2 and Night 3 simulate operational nights with telescope alignment calibration at the beginning of Night 2. Our optical model currently includes the global motion of M1, M2, and M3, capturing the largest effects that can be corrected by a low-order wavefront sensor. Future work will include individual segment motions that the M1 control system (M1CS) will correct in practice using segment edge sensors and segment position actuators. The M1CS residual shape will largely be uncorrected by the OIWFS and will likely be an additional source of noise in the simulation.

Figure 1 shows the rigid-body state time series for simulated operational Night 2. Note that the translational motions are larger than the rotational motions. This is to be expected since the telescope temperature is preconditioned while pointing at the horizon during the day. This causes a thermal gradient along the gravity direction (here y-direction in the global coordinate frame) and along the optical axis (z-direction in the global coordinate frame) to be dissipated throughout the night. Also note that we simulate the Alignment and Phasing System (APS) telescope alignment at the start of Night 2 by zeroing out the initial rigid-body states. Night 3 is then calibrated using this same set of values, simulating a night when APS is not run to calibrate the telescope alignment at the start of the night.

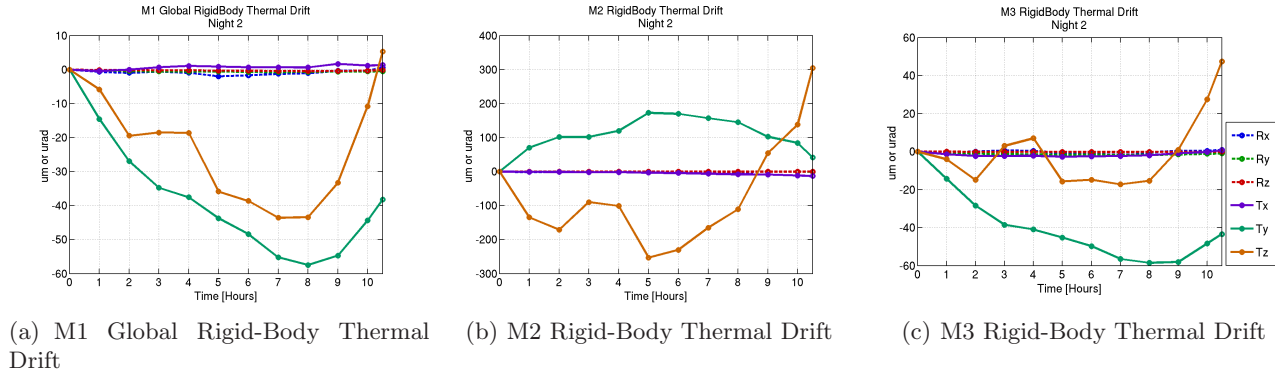


Figure 1. TMT mirror rigid-body time series due to thermal misalignment for operational Night 2. (Note y-axis scale difference.) R_i are rotations and T_i are translations in x, y, and z directions of the global coordinate frame.

3. WAVEFRONT SENSING

3.1 Optical Model

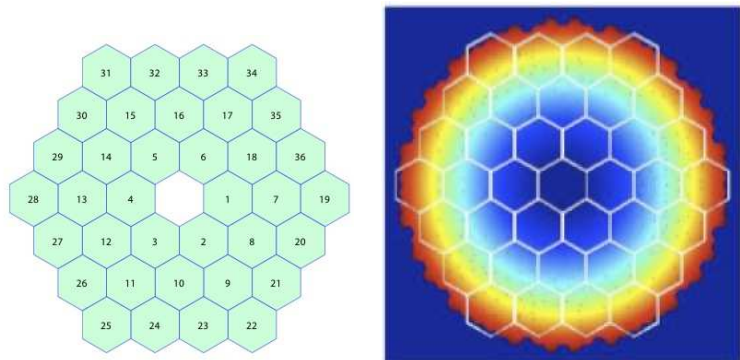
Using the optical model that we have previously developed for TMT systems engineering performance and sensitivity analyses, we can rapidly generating exit-pupil phase maps for rigid-body and mirror surface errors.⁶ The rigid-body state output of the TMT thermal and structural models are used as an input to generate phase map array time series simulating an observational night. These wavefront maps provide an input to a Matlab (The Mathworks, Inc.) based OIWFS model and to optical wavefront and image quality metric calculations, such as the rms wavefront error (WFE), PSSN, telescope pointing error, plate scale distortion, and exit pupil shear. Section 4.2 describes these optical metrics in further detail.

Although the optical model has the capability of generating phase maps at much higher resolution, for these OIWFS simulations we consider phases maps that are 512 pixels square with 4/64m sampling per pixel. This approximation is acceptable for the low-order wavefront errors induced by telescope misalignment because the PSSN sensitivity to phase map sampling is reduced for low spatial frequency errors across the pupil. Telescope PSFs are generated using Nyquist sampled FFTs at a wavelength of 500nm and an atmosphere r_0 equal to 200mm at the zenith.

3.2 On-Instrument Wavefront Sensor

A Shack Hartmann wavefront sensor (SH WFS) measures the average wavefront slope over each subaperture of the sampled wavefront defined by an array of lenslets positioned in the pupil-plane. This On-Instrument Wavefront Sensor (OIWFS) is mounted within the seeing limited instrument measuring the low-order telescope aberrations caused by M1, M2, and M3 misalignment. Wavefront sensing measurements can be used to maintain appropriate telescope alignment and wavefront quality by averaging to reduce atmospheric noise and sending corrections at a slow update rate (~ 5 mins sampling) throughout the night. To sense low-order spatial frequencies such as the second and third order aberrations, at least seven samples across the pupil are necessary; therefore, we have modeled a simple 3-ring hexagonal lenslet array WFS. Defining the formal requirements for such a WFS remains an item of future work for the project. This simplified design has the capability of demonstrating the OIWFS concept and setting approximate baseline parameters for the system. Figure 2 shows the configuration of the 3-ring lenslet array and the wavefront sampling across the phase map.

To simulate the OIWFS design described above, the telescope wavefront is divided up to include the region that is unique to each hexagonal lenslet. The slope is calculated using a least squares fit of tip and tilt across the hexagon. This simplification is made rather than propagating each lenslet's phase to a detector because a specific OIWFS design is not available and with such a large portion of the 30m pupil sampled by each hexagon, there should be ample star light available for spot centroiding on the pixel array. As a baseline case the OIWFS is positioned at the on-axis field point. Section 6.1 describes a simulation where multiple OIWFS were positioned across the telescope field-of-view (FoV) with only a slight increase in performance.



(a) 3-ring hexagonal lenslet array (b) OIWFS lenslets sampled over TMT exit pupil wavefront

Figure 2. OIWFS design baseline

3.3 Measurement Noise

We currently consider the effect of integrating over the atmosphere as the dominant source of measurement noise since the OIWFS measures star light through random atmosphere over a finite exposure time. Chanan, et al.⁷ have found that the Atmospheric Phase Residual Noise is the most dominant error source in the Phasing Camera System (PCS)⁸ of the Keck Telescopes. They have also predicted the measurement uncertainties of APS based upon empirical data from PCS, scaling them as appropriate to TMT. We have implemented this noise using the same method that our optical model uses to implement APS atmospheric residual error, using a Zernike atmospheric decomposition that decreases with the square-root of time as described by Chanan. For each wavefront measurement we include a phase error, scaling 1000 Zernikes for the atmospheric distribution and exposure time. The atmospheric noise is assumed to be independent between OIWFS and wavefront control time.

4. WAVEFRONT CONTROL

4.1 Control Model

To correct for system disturbances measured by the OIWFS, we currently consider a Type-1 servo controller with velocity control. This controller fundamentally seeks to generate a set of M2 rigid-body commands to minimize the WFS slope difference between the measured and target slopes. We have conducted a control DoF parameter study, described in Section 6.1, and adopted an M2 translation DoF control scenario as a baseline. The Type-1 servo measures the mean disturbance drift values for the measurements taken during each exposure time for latency consideration and therefore sends a velocity command to M2 for each control period.

Figure 3(a) shows the wavefront sensing and control loop architecture employed. The thermal disturbance is added to the telescope state, which is sensed by the OIWFS after averaging over the atmosphere. The measured spot positions are fed into the control algorithm, which updates the M2 commands for the current control period. As these M2 translation velocity commands are introduced onto the telescope, the OIWFS averages over the atmosphere, recording the measured spot positions and feeds this information for the controller to calculate an updated command set. This control process is shown in Figure 3(b) for an arbitrary disturbance profile. The mean system perturbation is measured over an exposure time, effectively using the perturbation velocity at the measurement instance (dashed-dotted green if colored). A velocity control command (dashed-dotted red if colored) is sent at the time marked control period (dashed purple if colored). This then corrects for the input perturbation (solid blue if colored) to the corrected state (solid black if colored) with velocity updates made to correct for perturbation profile changes. Note that this controlled state is subject to rapid fluctuations in the the disturbance slope, but that the TMT thermal disturbance inputs described in Section 2 do not change rapidly.

Some assumptions that we currently include in this wavefront control implementation relate to the precision of the control matrix and computation time. We assume that the rigid-body sensitivity matrix to M2 motion is known without error and therefore introduces zero error into the control matrix. This sensitivity can be initially calibrated with optical modeling and updated with system measurements in practice. The control solution computation time and actuator movement time are both assumed to be very small relative to the exposure time. This effectively assumes that the control iteration time is equal to the exposure time. Subimage motion due to telescope aberration changing during each exposure is also currently ignored.

4.2 Optical Metrics

To evaluate OIWFS performance our simulation records both optical wavefront and image performance metrics across the telescope FoV. The wavefront at the telescope exit pupil is measured at the off-axis field points shown in Figure 4. We evaluate 17 field points over the unvignetted 15 arcmin TMT FoV. For each measurement instance, the simulation records the root-mean-square and peak-to-valley wavefront error and a Zernike decomposition of the ΔOPD , which is the difference between the perturbed and unperturbed or target wavefront and reported in nanometers (nm). The PSSN is evaluated from PSFs generated from this same ΔOPD , using the unperturbed wavefront at each field point for normalization as described by Seo.¹⁻³ We then report the statistical mean, mean minus standard deviation, and minimum PSSN value over the 17 field points through the time series. The exit pupil shear records the motion of the exit pupil vertex point in the plane perpendicular to the optical

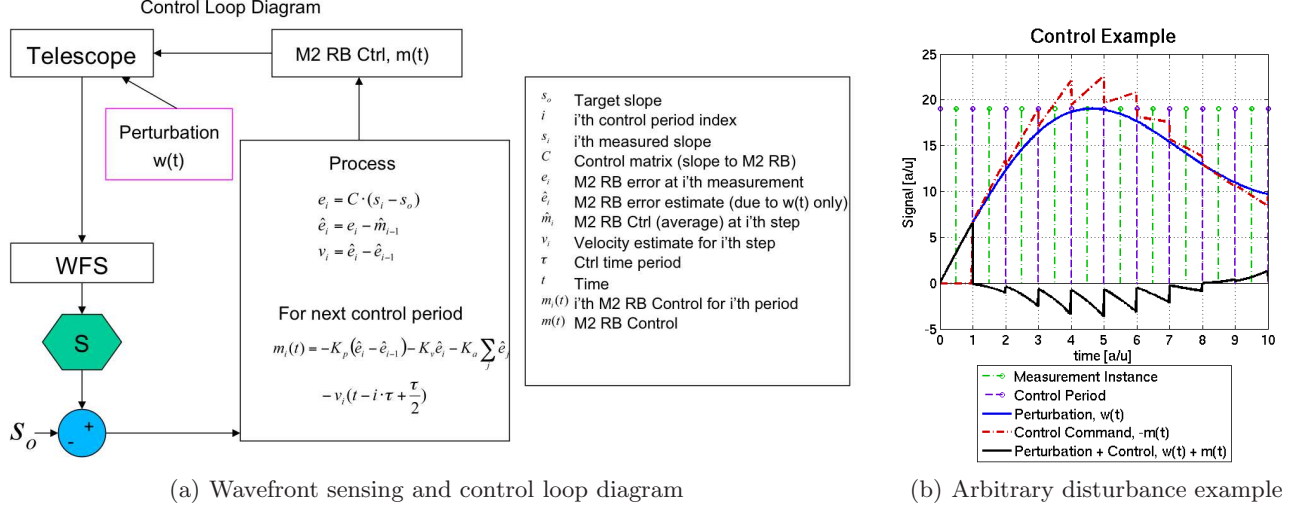


Figure 3. Control loop diagram and theoretical perturbation control example.

axis. This motion is recorded in microns (μm) of motion at the exit pupil, which is $\sim 3.09\text{m}$ in diameter. The telescope pointing error and plate scale distortion are calculated by tracing a set of rays to the image plane for each field position and recording their centroid position at each field. The pointing error is then equal to the motion of the on-axis field point rays scaled to be on-sky and reported in units of milli-arcseconds (mas). The plate scale distortion then subtracts this common motion from each bundle of rays, differences the perturbed and unperturbed motion, then normalizes to the mean image spot position reported in parts-per-million (ppm).

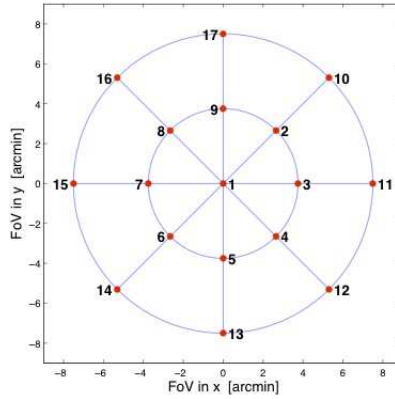


Figure 4. Optical metric calculation locations across TMT unvignetted FoV.

5. BASELINE SIMULATION CASE

To answer the question proposed by this study of whether an OIWFS can maintain the TMT wavefront throughout the observing night, we first implement the simplest case. That is, we position one OIWFS as described in Section 3.2 at the center point within the field of view and initiate the wavefront controller as described in Section 4.1. We find that this single OIWFS performs much better than the basic LUT concept does.

Figure 7 shows the performance results for the uncontrolled thermal disturbance case, control without noise, and control including atmospheric noise. The single WFS on-axis corrects the rms WFE from $7\mu\text{m}$ to less than 600nm . It maintains the mean PSSN to within 0.9986, the mean minus sigma to 0.9965, and gives a value of 0.9855 at the worst point. The pointing error is corrected from 838mas to 703mas , plate scale distortion from

27ppm to 17ppm, and the pupil shift from $170\mu\text{m}$ to within $117\mu\text{m}$. This single OIWFS configuration meets the TMT system engineering requirements for each tracked optical metric.

The image quality improvement is obtained by controlling M2 translations through velocity control with an update rate of 300secs of atmospheric integration. We observe that the performance is independent of FoV across the 15arcmin unvignetted telescope field. This suggests, and we show in the following Section 6.1, that positioning additional OIWFS within the FoV and using the knowledge from multiple field points does not improve telescope performance significantly. This performance is obtained using the simple low-order SH WFS described in Section 3.2. Incremental performance improvement could be obtained by increasing the number of lenslets sampled across the pupil, with a loss of sky coverage. A much higher order WFS would be necessary to correct for segment level drifts that are uncontrolled by M1CS, such as focus mode. Improvement to this simple OIWFS design and implementation of a high-order WFS lay outside the scope of this study.

6. PARAMETER STUDIES

6.1 Controlled Degrees of Freedom

The simulation framework that we have implemented and described allows us to conduct parametric studies relating to WFS configuration and controlled DoFs. We have shown that an OIWFS can correct for the thermal disturbance errors seen by the telescope throughout a night of observation and meet the telescope requirements. This suggests the question of whether multiple OIWFSs positioned across the unvignetted FoV can improve the telescope performance. We implement this multiple OIWFS configuration as shown in Figure 5. Here we have positioned three additional WFSs at 0.7 times the unvignetted FoV limit, $\sim 5.25\text{arcmin}$, to provide supplementary field-dependent wavefront information. Another interesting study relates to whether controlling M2 rotation instead of, or in addition to, the translation control can improve performance.

Table 1. OIWFS configuration and controlled DoF parameter study results.

	# of WFS Config.	Controlled M2 DoF	PSSN			Pointing Error [mas]	Plate Scale Dist. [ppm]	Pupil Shift [μm]
			μ^*	$\mu - \sigma$	min			
0	None	None	0.6694	0.4768	0.3445	838	27	170
1	4	[Rx,Ry,Rz,Tx,Ty,Tz]**	0.9991	0.9924	0.9504	5472	119	627
2	4	[Rx,Ry,-,-,Tz]	0.9995	0.9959	0.9829	921	22	177
3	4	[-,-,Tx,Ty,Tz]	0.9996	0.9987	0.9917	571	13	86
4	1	[Rx,Ry,-,-,Tz]	0.9984	0.9944	0.9807	938	22	177
5 [†]	1	[-,-,Tx,Ty,Tz]	0.9986	0.9965	0.9855	703	17	117

[†] Baseline Case

* 3 PSSN values are recorded: mean (μ), mean - standard deviation ($\mu - \sigma$), and minimum (min)

** R_i are rotations and T_i are translations in x, y, and z directions of the global coordinate frame.

Table 1 summarizes the results of this parametric study. The baseline simulation case is shown in the marked Row 5, of 1 OIWFS positioned at the center field point with M2 translation control only. Row 4 shows performance results for this same single OIWFS but employs M2 x and y-rotation control and piston correction. This configuration responds slightly worse in terms of image performance and also degrades the telescope pointing error, plate scale distortion, and pupil shift. Although the x and y-rotation DoFs are degenerate from the x and y-translation DoFs for M2, correcting for the translation performs better since the thermal disturbance inputs are translation dominant.

Rows 1-3 of Table 1 show the performance results for 4 OIWFS positioned across the field. In Case 3, where additional knowledge is available for the same translation only control case, each metric benefits slightly from the added measurements. Case 2 provides supplementary knowledge across the field and controls M2 x and y-rotation instead of translation. Here the image quality is slightly improved as compared to Case 4, although the pointing error and pupil shift again degrade. When combining both effects in Case 1, allowing for additional wavefront knowledge but controlling degenerate modes of M2 motion, the performance in terms of each metric degrades. This is because the uncorrelated atmospheric noise measured by each WFS adds to 5 controlled DoFs rather than only 3. This Case 1 does have superior control in the absence of noise.

Since a single OIWFS with M2 translation control performs just as well (or better) than 4 OIWFS positioned across the field at 1/4 of the cost and since the thermal disturbance is translation dominant, we recommend the baseline case as noted.

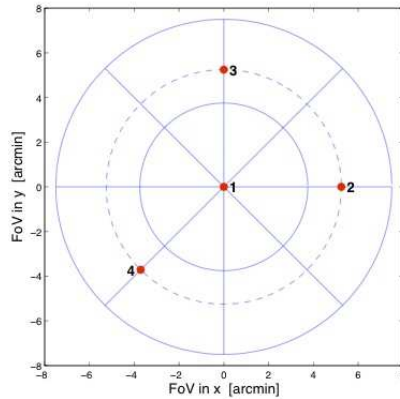


Figure 5. Multiple OIWFS Configuration

6.2 Integration Time

We have conducted a parameter study to estimate the optimum integration time for the OIWFS configuration that we have described. In a noiseless case, reducing the integration time will always maximize performance. However, when noise is present, this is not true because the atmospheric measurement noise then dominates over the system drift for smaller integration times. An optimum time will balance the system disturbance drift and the atmospheric noise integration. By varying the integration time parameter within our OIWFS simulation, we can determine the optimum balance between the two. Figure 6 shows the results of varying this parameter within our simulation. Three control modes are shown with and without atmospheric noise, with Mode 1 denoting the configuration shown in Row 1 of Table 1 and so on. The curve labeled Mode 5 then denotes the baseline case that we have described. For this Case 5 with noise included (Ctrl Mode 5, (Atm. Noise)) the optimal integration time is approximately 300sec. This is the value that we have set as the baseline integration time for our simulations and compares well with the findings of the APS group.

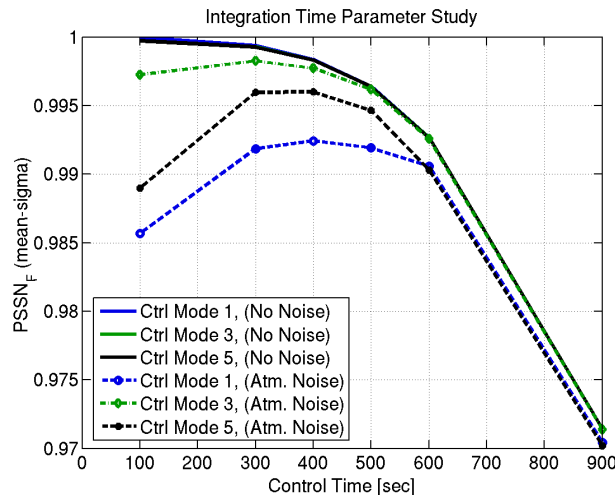


Figure 6. Mean minus standard deviation PSSN performance vs. OIWFS integration time with and without atmospheric noise included. The optimum integration time is found at ~ 300 secs (5mins) where the PSSN is at a maximum for the baseline simulation Case 5 (Ctrl Mode 5, (Atm. Noise)).

7. CONCLUSION

In this study we have presented a solution to correct for thermally induced misalignment of TMT. We have shown that adequate correction of these thermal effects using a look-up-table approach would prove to be challenging. This wavefront maintenance can be achieved using a single OIWFS positioned at the center of the telescope FoV, correcting for the sensed misalignments with velocity commands of M2 translation. We have investigated the benefits of increasing the number of wavefront sensors and found that a single OIWFS performs just as well (or better) than multiple OIWFS do in terms of image quality evaluated using PSSN. The pointing error, plate scale distortion, and pupil shift do improve with the supplementary wavefront measurements. However, a single OIWFS meets the system engineering requirements for these terms. Since the thermal alignment errors throughout the observation night are translation dominant in each simulation case, controlling the translation DoFs of M2 yield improved performance over rotation control. These OIWFS simulations also show that the optimum atmospheric integration and sampling time is ~ 300 secs, which compares well with the findings of the APS studies conducted for TMT.

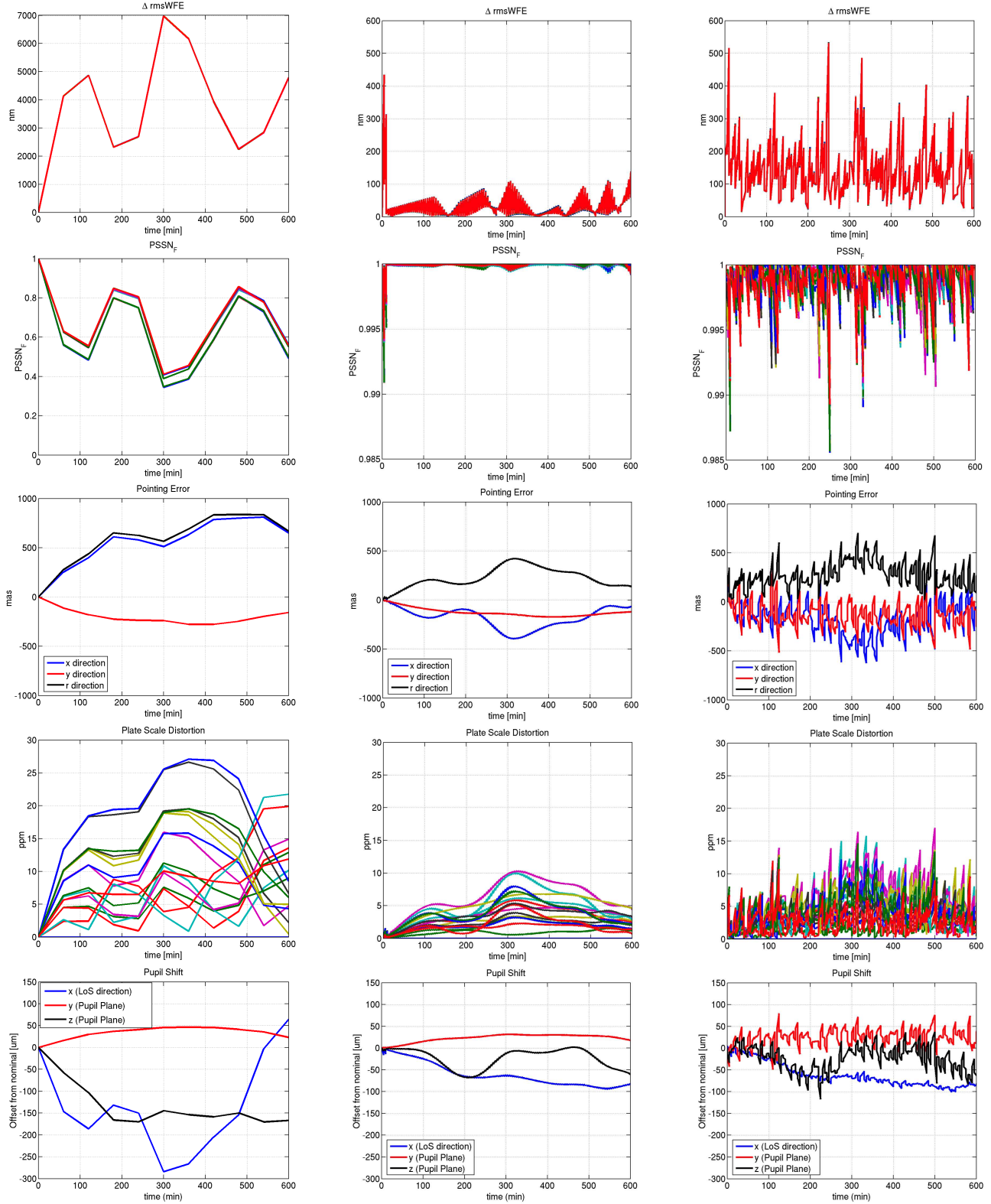
Future work for these OIWFS simulations relate to including other environmental errors and simulating the OIWFS within the seeing limited TMT instrument MOBIE. This instrument's field is positioned off-axis and would therefore place an OIWFS near its operating FoV. We can quickly simulate the image quality effects on this implementation. We also plan to include gravity misalignment effects and M1CS residual error as additional system disturbances. These will include the effects of segment in-plane motion and M1CS sensor noise. These terms will be an added source of noise to the low order WFS that we have described, but should not impact the feasibility of the OIWFS solution to wavefront maintenance.

ACKNOWLEDGMENTS

This research was carried out in part at the Jet Propulsion Laboratory, California Institute of Technology, and was sponsored by the California Institute of Technology and the National Aeronautics and Space Administration. The authors gratefully acknowledge the support of the TMT partner institutions. They are the Association of Canadian Universities for Research in Astronomy (ACURA), the California Institute of Technology and the University of California. This work was supported as well by the Gordon and Betty Moore Foundation, the Canada Foundation for Innovation, the Ontario Ministry of Research and Innovation, the National Research Council of Canada, the Natural Sciences and Engineering Research Council of Canada, the British Columbia Knowledge Development Fund, the Association of Universities for Research in Astronomy (AURA) and the U.S. National Science Foundation.

REFERENCES

1. B.-J. Seo, C. Nissly, G. Angeli, B. Ellerbroek, J. Nelson, N. Sigrist, and M. Troy, "Analysis of Normalized Point Source Sensitivity as a performance metric for the Thirty Meter Telescope," *Proc. SPIE* **7017**, p. 70170T, June 2008.
2. B.-J. Seo, C. Nissly, G. Angeli, B. Ellerbroek, J. Nelson, N. Sigrist, and M. Troy, "Analysis of Normalized Point Source Sensitivity as performance metric for large telescopes," *Applied Optics* **48**, pp. 5997–6007, 2009.
3. B. Seo, C. Nissly, M. Troy, and G. Angeli, "Normalized point source sensitivity for off-axis optical performance evaluation of the Thirty Meter Telescope," *Proc. SPIE* **7738**, June 2010.
4. K. Vogiatzis, "Thermal modeling environment for TMT," *Proc. SPIE* **7738**, June 2010.
5. M. Cho, A. Corredor, K. Vogiatzis, and G. Angeli, "Thermal performance prediction of the TMT telescope structure," *Proc. SPIE* **7427**, August 2009.
6. C. Nissly, B. Seo, M. Troy, G. Angeli, J. Angione, I. Crossfield, B. Ellerbroek, L. Gilles, and N. Sigrist, "High-resolution optical modeling of the Thirty Meter Telescope for systematic performance trades," *Proc. SPIE* **7017**, p. 70170U, June 2008.
7. G. Chanan, M. Troy, and I. Crossfield, "Predicted measurement accuracy of the TMT Alignment and Phasing System," *TMT Project Communication* **TMT.CTR.PRE.07.007.REL01**, Feb 2007.
8. G. Chanan, "Design of the Keck Observatory alignment camera," *Proc. SPIE* **1036**, p. 59, 1988.



(a) Open loop without noise

(b) Closed loop without noise

(c) Closed loop with atmospheric noise

Figure 7. Baseline simulation case performance at field points noted in Figure 4. (Note y-axis scale difference for rms wavefront error and PSSN metrics between cases.)